JOURNAL OF CATALYSIS 87, 179–195 (1984)

Spectroscopic and Catalytic Studies on Metal Carbonyl Clusters Supported on Cab-O-Sil

II. Impregnation and Decomposition of $Ru_3(CO)_{12}$ and the Mixture of $Ru_3(CO)_{12}$ and $Fe_3(CO)_{12}$

Z. SCHAY, K. LÁZÁR, J. MINK, AND L. GUCZI*

Institute of Isotopes of the Hungarian Academy of Sciences, P.O. Box 77, H-1525 Budapest, Hungary

Received September 9, 1982; revised February 23, 1983

The behavior of $Ru_3(CO)_{12}$ (I), $H_2Ru_3Fe(CO)_{12}$ (II), a 1 : 1 $Ru_3(CO)_{12}$ and $Fe_3(CO)_{12}$ mixture (III), $RuFe_2(CO)_{12}$ (IV), and $Fe_3(CO)_{12}$ (V) deposited on Cab-O-Sil HS-5 has been compared. (III) and (V) have been studied by Mössbauer spectroscopy and by ir-spectroscopy, and (I)-(V) by temperature-programmed decomposition (TPDC) and temperature-programmed reduction (TPR). Decomposition, which is faster in hydrogen than in helium or in vacuum, and is reversible below 400 K, is normally faster for (V) than for (I). At low temperature, CO ligands leave the metal carbonyl cluster (MCC) in one step for (V), whereas they are decomposed stepwise via the formation of subcarbonyl species for (I). In this range the formation of $Ru_3(CO)_3$ species has been verified. On decomposition of (V), there is some CO adsorption, as indicated by ir spectroscopy and low catalytic activity. This increases when decomposition occurs in helium, and is attributed to the smaller particles stabilized by the metal–carbon species, formed from CO during the decomposition. For (I), decomposition results in a slight oxidation, indicated by weak ir bands in the range of 2100–2140 cm^{-1}. Interaction between Fe and Ru in (III) does not occur in the impregnated phase, but develops during the decomposition, which starts with $Fe_3(CO)_{12}$ decomposition and thereby influences the decomposition of $Ru_3(CO)_{12}$. However, reduction of iron is also facilitated by the presence of ruthenium, as indicated by Mössbauer spectroscopy. The general feature revealed during decomposition in helium, i.e., the increase of surface carbon, is also operative here, and thus the dispersion of the metal is higher than for decomposition in hydrogen. The mechanism of the decomposition is discussed in terms of the formation of subcarbonyl species for Ru-containing samples and the formation of surface carbon is also considered. The mechanism and possible reaction pathways are given.

INTRODUCTION

In Part I (*1*) the mode of interaction of $Fe_3(CO)_{12}$ with Cab-O-Sil has been reported. In contrast with literature data (*2*), special interactions between the carbonyl cluster and the support have been established. Because of the well defined interaction between iron and ruthenium, which has been shown by catalytic studies (*3*), investigations on the interaction between the ruthenium clusters and Cab-O-Sil, as well as between the two metals, seem interesting.

The question now arises as to the stage of catalyst preparation, i.e., the step in the sequence of the decomposition of the metal carbonyl clusters, at which the metal-metal interaction is developed. Neither the application of ir techniques alone on supported $Fe_3(CO)_{12}$ (*4, 5*), and $Ru_3(CO)_{12}$ (*2, 6*), nor studying the effects of the support (*2, 3, 6–10*) have answered this question.

The fundamental work of Kuznetsov *et al.* (*2*) on the interaction between ruthenium carbonyl clusters of different nuclearity and alumina showed that interaction mainly depends on the heat pretreatment given to the alumina, consequently on the

* To whom correspondence should be addressed.

0021-9517/84 $3.00

number of OH groups and Lewis acid centers on the surface. With silica, however, they found weak interaction between the clusters and a silica gel surface due to dehydroxylation. The statements mentioned were in agreement with those obtained on rhodium carbonyl cluster deposited on silica gel and alumina (*11–13*). In those studies, the formation of subcarbonyl species was observed during the decomposition and the influence of ambient atmosphere on the reversibility of decomposition was also studied.

In Part I (*1*) it was established that interaction between $Fe_3(CO)_{12}$ and Cab-O-Sil support developed and that it took the form of electron transfer from the support oxygen atoms to the metal framework, and also to interaction of the type Fe–CO ··· HO–Si.

The main goal of the present work is to gain information about (i) the temperature up to which the metallic framework exists in an M_3 carbonyl structure during decomposition, (ii) the stage of preparation at which iron–ruthenium interaction is developed, (iii) the mechanism of carbon formation and removal during the decomposition, and (iv) the correlation between chemisorption and catalytic activity for the CO + H_2 reaction. Several different experimental techniques are applied, such as the detailed analysis of the gas phase by GC and MS, the structure of the solid phase by Mössbauer spectroscopy, and the structure of the gas–solid interface by ir spectroscopy.

EXPERIMENTAL

Materials. $Fe_3(CO)_{12}$ and $Ru_3(CO)_{12}$ were purchased from Strem Chemicals. ^{57}Fe-labeled $Fe_3(CO)_{12}$ was synthesized by the method described in Part I (*1*). In the preparation of $Fe_2Ru(CO)_{12}$ and $H_2FeRu_3(CO)_{13}$ a different method was followed (*14*). The following samples were prepared by the method reported in Part I (*1*): $Ru_3(CO)_{12}$ on Cab-O-Sil (sample I); $H_2Ru_3Fe(CO)_{13}$ on Cab-O-Sil (sample II); a mixture of $Fe_3(CO)_{12}$ and $Ru_3(CO)_{12}$ on Cab-O-Sil (sample III); $RuFe_2(CO)_{12}$ on Cab-O-Sil (sample IV); and $Fe_3(CO)_{12}$ on Cab-O-Sil (sample V). Unless indicated elsewhere, the total metal loading is 1 wt%. The mixture sample III contains both metals in the same weight percentage.

Cab-O-Sil HS-5 was obtained from Cabot Corporation (Boston). All gases used during Mössbauer and ir studies, as well as in temperature-programmed decomposition and temperature-programmed reaction measurements, were purified by passing through a Deoxo unit followed by molecular sieve A5.

Apparatus. Infrared and Mössbauer measuring techniques were described in Part I (*1*). Mössbauer spectroscopy is devoted to the iron-containing catalysts prepared from ^{57}Fe-labeled MCC. Unfortunately, the bimetallic catalysts prepared from bimetallic clusters could not be studied by Mössbauer spectroscopy, due to the lack of ^{57}Fe-labeled material.

Infrared measurements were carried out on a DIGILAB FTS-14 Fourier Transform spectrometer and on a DIGILAB FTS-20C machine equipped with a Nova-3 computer and a dual drive, 10 megabyte disk system.

Temperature programmed decomposition (TPDC) of the supported clusters was carried out in a flow system. Helium or hydrogen was applied as carrier gas and the effluent was fed to a thermal conductivity cell (TC) or flame ionization detector (FID). In the former case, the total amount of decomposition products was measured, whereas with FID only hydrocarbons are detected. In some cases, the effluent passed through a nickel catalyst heated to 630 K to convert the CO and CO_2 into methane and thus the total products formed could be measured. Part of the effluent gas could also be analyzed by leaking it into a mass spectrometer Type MS 10 C2 (Kratos). Thus CO, CO_2, and methane could be analyzed along the whole temperature range.

The influence of the solvent on decomposition was studied by a DuPont 21-490 B GC-MS machine. The effluent of the de-

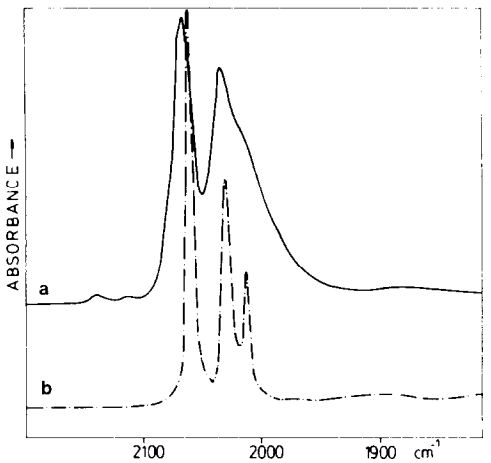

FIG. 1. Infrared spectra of $Ru_3(CO)_{12}$. (a) In hexane, (b) impregnated on Cab-O-Sil.

composition products was introduced to a GC column, and after separation the products were identified in the mass spectrometer.

The flow system applied to TPDC was also used for measuring CO adsorption and for temperature-programmed reaction (TPR) of CO, which is regarded as a simple test for the catalysts obtained. Here the reaction took place in hydrogen and only hydrocarbon products were analyzed by FID.

RESULTS

$Ru_3(CO)_{12}$ on Cab-O-Sil Impregnation

Infrared spectra (Fig. 1 and Table 1) showed that the impregnation of $Ru_3(CO)_{12}$ was accompanied by a shift in terminal carbonyl bands (3–4 cm^{-1}) which is smaller than that for sample (V). Here, line broadening was also observed, and, similar to iron, a small number of CO molecules are bonded to oxidized ruthenium, as characterized by the band above 2100 cm^{-1} frequency.

It should be mentioned that weak bands appeared at 2934 and 2860 cm^{-1} on all impregnated samples, giving an indication of the presence of trace amounts of hexane left after the preparation of the sample.

TABLE 1

Positions of ir Absorption Bands (in cm^{-1}) for $Ru_3(CO)_{12}$ in Hexane Solution and for $Ru_3(CO)_{12}$/Cab-O-Sil

$Ru_3(CO)_{12}$ (*n*-hexane solution)	$Ru_3(CO)_{12}$/Cab-O-Sil (room temperature)	Assignments
	2140 w	CO bonded to
	2120 vw	the oxidized
2100 vw	2112 vvw	$Ru^{\delta+}$
	2070 sh	
2061 vs	2065 vs	
2031 s	2034 s	Terminal CO
2012 s,m	2015 sh	stretching
1972 vvw	1975 sh	mode
	~1850 vw,b	

Thermal Decomposition

Two well-defined temperature ranges can be distinguished during decomposition of sample (I) in H_2. Below 400 K, cluster character is retained, whereas at higher temperature, CO bands resemble to those of chemisorbed CO on a Ru surface (*15*). In Fig. 2, a three-dimensional plot of decomposition is presented. At as low temperature as 310 K, there is chemical change accompanied by the formation of $Ru_3(CO)_{12-n}$ species and characterized both by the development of bands at 2080 and 2003 cm^{-1} and by the disappearance of the band at 2034 cm^{-1}. In Fig. 3 spectra of sample (I) decomposed in vacuum are presented. The spectra resemble those obtained for sample (III), which will be discussed later. At higher temperatures (>400 K) the cluster character completely vanishes (see Fig. 4) and the appearance of a broad band at 1980 cm^{-1} is observed. The intensity of this band slightly decreases up to 500 K but can still be observed at 780 K. It strongly overlaps the uncompensated band of the support; thus its interpretation is difficult and is omitted here.

It should be mentioned that the $Ru_3(CO)_{12-n}$ structure on the surface can be repeatedly produced when decomposition is ceased at 410 K and the sample is cooled to room temperature in the presence of CO. When sample (I) is treated at higher temperature, the repeated CO uptake results in

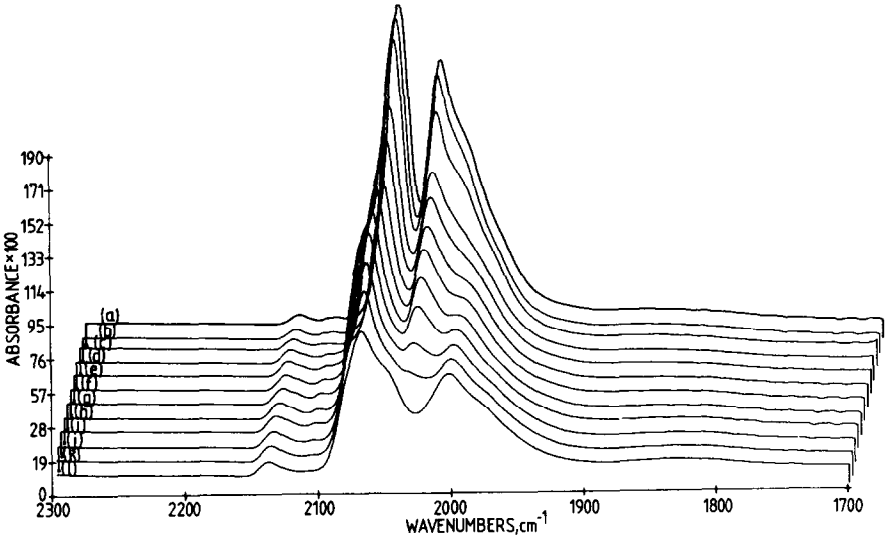

FIG. 2. Three-dimensional plot of thermal decomposition for $Ru_3(CO)_{12}$/Cab-O-Sil under stream of H_2. (a) 302 K under vacuum; (b) 302 K under H_2; (c) 311 K; (d) 320 K; (e) 331 K; (f) 343 K; (g) 353 K; (h) 362 K; (i) 368 K; (j) 378 K; (k) 390 K; (l) 401 K.

a spectrum which resembles CO chemisorbed on a Ru surface with bands at 2133, 2072, and 2010 cm^{-1} (*15*). The characteristics of decomposition are summarized in Table 2.

$Fe_3(CO)_{12}$ + $Ru_3(CO)_{12}$/Cab-O-Sil Impregnation

The ir spectra of a mixture of $Fe_3(CO)_{12}$ and $Ru_3(CO)_{12}$ deposited on Cab-O-Sil are

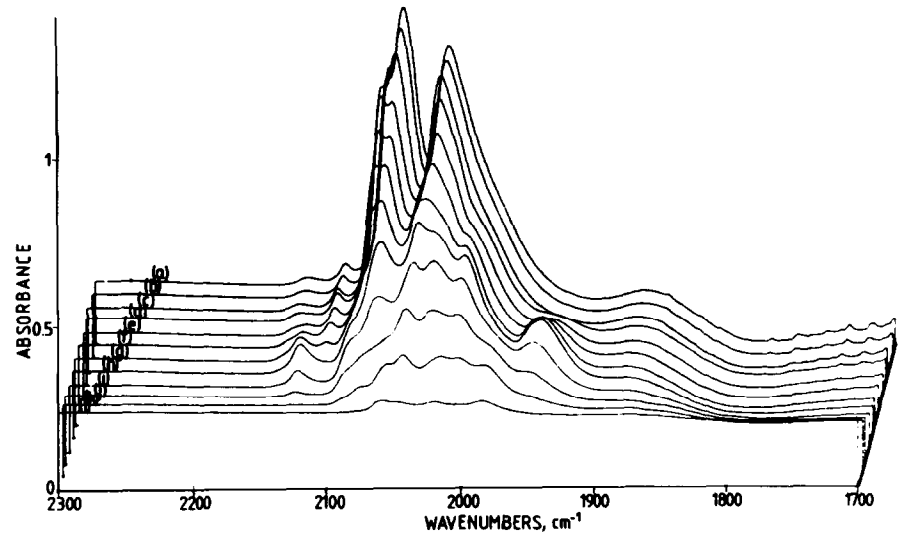

FIG. 3. Three-dimensional plot of thermal decomposition of $Ru_3(CO)_{12}$ on Cab-O-Sil under vacuum. (a) 303 K; (b) 319 K; (c) 336 K; (d) 369 K; (e) 387 K; (f) 400 K; (g) 415 K; (h) 460 K; (i) 514 K; (j) 562 K; (k) 606 K; (l) 662 K.

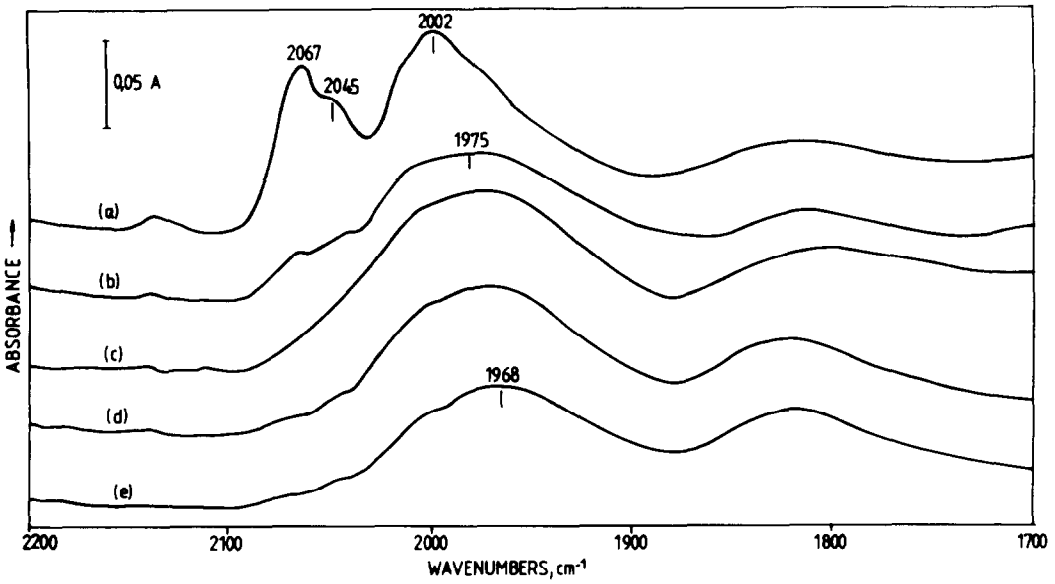

FIG. 4. Infrared spectra of $Ru_3(CO)_{12}$/Cab-O-Sil decomposed under H_2 in temperature range 401–498 K. (a) 401 K; (b) 410 K; (c) 444 K; (d) 475 K; (e) 498 K.

shown in Fig. 5 (curve (a)). It is inferred that there is no interaction in the impregnated stage because the ir spectrum of the mixture is practically the sum of the two separate spectra measured with the individual components. Bands at 2057, 1864, and 1806 cm^{-1} certainly belong to iron dodecacarbonyl, but the others are overlapped (see Table 3).

Mössbauer spectra of the impregnated sample (III) very much resemble those of sample (V) (*1*), i.e., a quadrupole doublet

TABLE 2

Characteristic Carbonyl Stretching Frequencies (in cm^{-1}) during Thermal Decomposition of $Ru_3(CO)_{12}$/Cab-O-Sil under H_2

$Ru_3(CO)_{12}$/Cab-O-Sil[a]	$Ru_3(CO)_{12-n}$/Cab-O-Sil[b]	$Ru_3(CO)_{12-m}$/Cab-O-Sil[c]	Ru/Cab-O-Sil[d]	Ru/Cab-O-Sil + CO
2140 w	2134 w			2133 m
2120 vw				
2112 vvw	2110 vvw			
	2080 sh	2080 vs		
2070 sh		2072 vs		2072 vs
2065 vs	2068 vs			
	2050 sh			
2034 s		2028 vs		
2015 sh				2010 s
	2003 s			
		1990 vw		
1975 sh	1975 sh		1975 s,b	

[a] Original supported cluster at 300 K.
[b] Partly decomposed cluster below 340 K.
[c] Further decomposition at temperature range 340–400 K, determined from ratio-recorded spectra, $m > n$.
[d] Decomposed cluster above 410 K, where the band is masked by a temperature-dependent silica band.
[e] Readsorption of CO at room temperature.

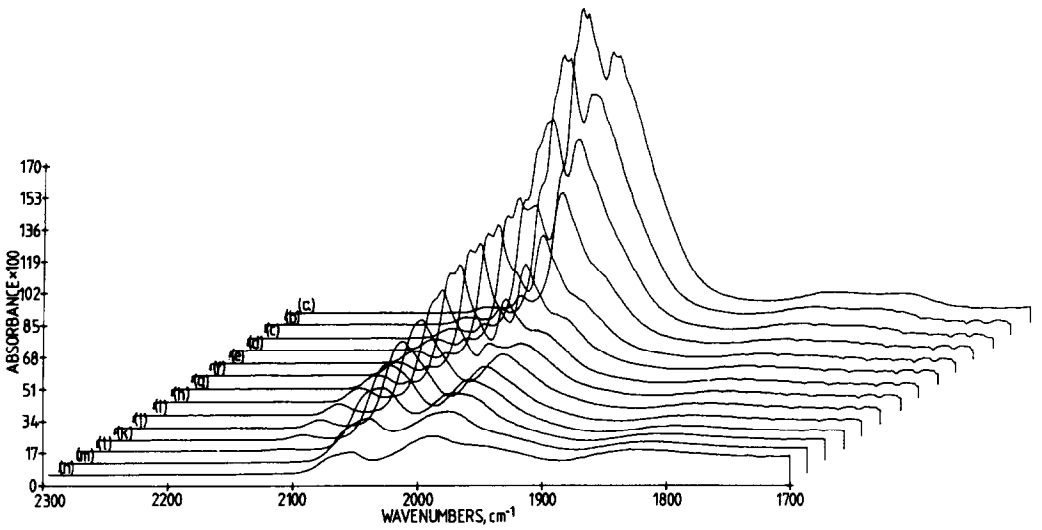

FIG. 5. Three-dimensional plot of thermal decomposition for $Ru_3(CO)_{12}$ + $Fe_3(CO)_{12}$ on Cab-O-Sil under stream of H_2. (a) 301 K; (b) 311 K; (c) 319 K; (d) 328 K; (e) 335 K; (f) 345 K; (g) 355 K; (h) 368 K; (i) 379 K; (j) 391 K; (k) 405 K; (l) 428 K; (m) 463 K; (n) 503 K.

was present (IS = 0.43 mm s^{-1} and QS = 0.95 mm s^{-1}) and oxidation of iron to form Fe^{2+} could not be measured up to 370 K.

Thermal Decomposition of Sample (III)

Infrared spectra of sample (III), decomposed in H_2, are presented in Fig. 5. Decomposition commences with fast CO removal [see spectra (a)–(f)]. About half of the CO is removed up to 340 K.

TABLE 3

Infrared Spectra of $Ru_3(CO)_{12}$ and $Fe_3(CO)_{12}$ Mixture Deposited on Cab-O-Sil

$Ru_3(CO)_{12}$ + $Fe_3(CO)_{12}$ on Cab-O-Sil at room temperature (cm^{-1})	Assignments[a]
2139 w	CO bonded to
2110 w	oxidized $M^{\delta+}$
2080 sh	
2068 sh	Terminal CO
2062 vvs	stretching mode
2057 sh	
2036 s	
~2015 sh	
1864 vw,b	Bridged CO
1806 vw,b	stretching mode

[a] For further assignments see text and Ref. (*15*).

This means that the process starts with decomposition of $Fe_3(CO)_{12}$. Later, at higher temperatures, the spectra are similar to those shown in Fig. 2 for $Ru_3(CO)_{12}$, i.e., $Ru_3(CO)_{12-n}$ is produced on the surface, with further decomposition to $Ru_3(CO)_{12-m}$ ($m > n$) up to 503 K, at which temperature the presence of CO ligands can still be detected. CO could be easily readsorbed, as indicated by the bands at 2136, 2072, and 2017 cm^{-1} on the sample heated up to 700 K (see Fig. 6).

A more complex picture is shown by the ir spectra for the decomposition of sample (III) in vacuum (Fig. 7). At 416 K, a new band at 2040 cm^{-1} is developed. The spectra measured up to 520 K are very similar to the spectra of the cluster at low temperature, but the presence of CO at 670 K is still detectable, in which case the spectra are very similar to those measured for linearly bonded CO on ruthenium.

CO readsorption can be seen in Fig. 6. On sample (III) (as mentioned for Fe/Cab-O-Sil, no CO adsorption was detected) a significant shift could be measured only at high wavenumbers. This may be due to the presence of iron in the system.

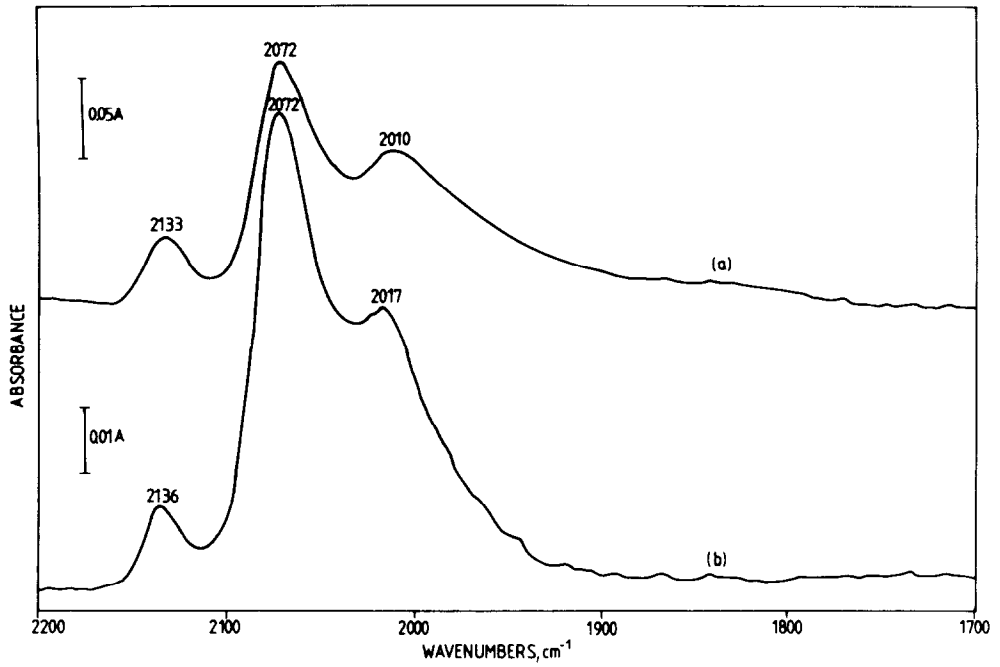

FIG. 6. Readsorption of CO on reduced supported clusters. (a) From $Ru_3(CO)_{12}$/Cab-O-Sil at 700 K under H_2, (b) from $Ru_3(CO)_{12}$ + $Fe_3(CO)_{12}$ on Cab-O-Sil at 700 K under H_2 after addition of 1 kPa CO at room temperature and evacuation.

Mössbauer spectra of sample (III) treated at 370 K gave a doublet with parameters of IS = 0.32 mm s^{-1} and QS = 1.01 mm s^{-1}. After 1 h heating in hydrogen at 470 K, Fe^{2+} and Fe^{3+} were observed and after 1 h reduction at 720 K in hydrogen, a small amount of superparamagnetic $Fe^{(0)}$ was also detected, as presented in Table 4.

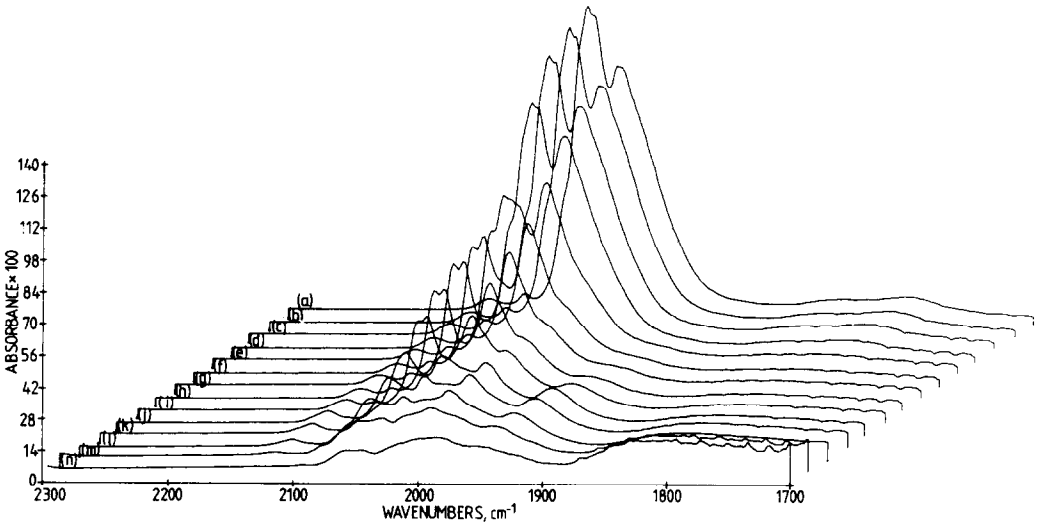

FIG. 7. Three-dimensional plot of thermal decomposition for $Fe_3(CO)_{12}$ + $Ru_3(CO)_{12}$ on Cab-O-Sil under vacuum treatment. (a) 298 K; (b) 311 K; (c) 323 K; (d) 338 K; (e) 351 K; (f) 363 K; (g) 373 K; (h) 387 K; (i) 403 K; (j) 416 K; (k) 446 K; (l) 473 K; (m) 523 K; (n) 573 K.

TABLE 4

Mössbauer Parameters of Sample (III) after 1 h Reduction in Hydrogen (Spectra Measured at 80 K)

Component	Temperature of heat treatment (K)							
	470				720			
	IS (mm s^{-1})	*QS* (mm s^{-1})	Ratio *R*	$\frac{\chi^2}{\langle\chi^2\rangle}$	*IS* (mm s^{-1})	*QS* (mm s^{-1})	Ratio *R*	$\frac{\chi^2}{\langle\chi^2\rangle}$
Fe^0	—	—	—		0.02	—	48[a]	
Fe^{2+}	1.14	2.29	38	16	1.16	1.91	10	2.7
Fe^{3+}	0.47	0.95	62		0.37	1.16	42	

Note. *IS*, isomer shift; *QS*, quadrupole splitting. *R* stands for the relative intensities (%). $\chi^2/\langle\chi^2\rangle$ characterizes the quality of fitting, its optimal value being between 1 and 2.

[a] 32% paramagnetic, 16% strongly magnetic.

Sample (III) showed similar behavior when treated in He. Decomposition at 420 K gave Fe^{2+} and Fe^{3+} components (see Fig. 8, curve (a)). At room temperature, a large fraction of the Fe^{2+} ions were oxidized (curve (b)). After the next treatment, performed at 670 K, the recorded spectrum showed mainly Fe^{2+} ions (curve (c)). After 24 h this component was partly converted to Fe^{3+} (curve (d)). All parameters are presented in Table 5. The totally oxidized sample is shown in curve (e).

TPDC and TPR Measurements for Samples (I) to (V)

As indicated in Part I (*1*), on decomposition part of the CO is converted into surface carbon, thereby influencing both the catalytic properties of the catalyst formed and the metal dispersion. The carbon cannot be measured by ir- or Mössbauer spectroscopy. In this section results on TPDC and TPR are presented and the formation of surface carbon will be examined.

Previous TPDC studies (*16, 17*) have indicated the overall characteristics of the decomposition obtained on the supported metal carbonyl clusters (I)–(V). Generally, at about 360 K a large peak appears which is mainly CO leaving the cluster. For (V), a second peak consisting of CH_4 appears above 630 K, while for clusters containing ruthenium ((I)–(IV)), a group of peaks appeared in the temperature range between 470 and 570 K. Here the main products are methane and a small amount of CO.

The analysis of the peaks by mass spectroscopy revealed some further interesting features of the decomposition. On the supported MCC with considerable iron content ((V) and (IV)), decomposed in He, a small hydrogen peak exists at around 370 K and continuously increases with rising temperature. Above 600 K, methane also increases

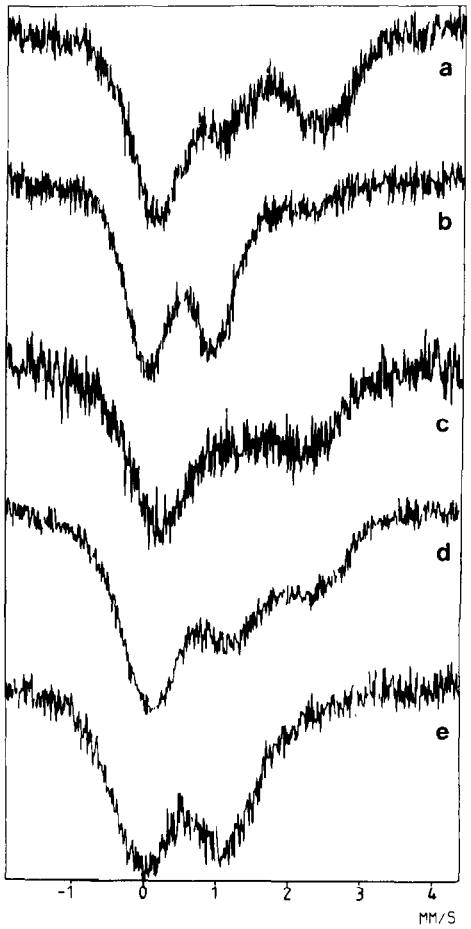

FIG. 8. Mössbauer spectra of Fe–Ru sample treated in helium and oxygen. (a) After decomposition in helium at 420 K, measured at 80 K, (b) sample (a) measured after 24 h at 300 K, (c) sample (b) after heating in helium at 670 K, measured at 80 K, (d) sample (c) measured after 24 h at 80 K, (e) sample (d) after 1 h treatment in oxygen atmosphere at 300 K, measured at 80 K.

TABLE 5

Mössbauer Parameters of Sample (III) after Treatments in Helium

Treatment		Temperature of measurement (K)	Component	*IS*	*QS*	*R*	$\frac{\chi^2}{\langle\chi^2\rangle}$
Temperature (K)	Duration (h)			(mm s^{-1})			
420	1.0	80	Fe^{2+}	1.10	2.31	57	1.08
			Fe^{3+}	0.48	0.86	43	
500	2.0	300	Fe^{2+}	1.11	2.10	13	1.35
			Fe^{3+}	0.33	0.94	87	
670	0.4	80	Fe^{2+}	1.17	2.09	57	1.42
			Fe^{3+}	0.60	1.05	43	
150	4.0	80	Fe^{2+}	1.12	2.23	33	1.14
			Fe^{3+}	0.53	1.16	67	

Note. IS, isomer shift; *QS*, quadrupole splitting. *R* stands for the relative intensities (%). $\chi^2/\langle\chi^2\rangle$ characterizes the quality of fitting, its optimal value being between 1 and 2.

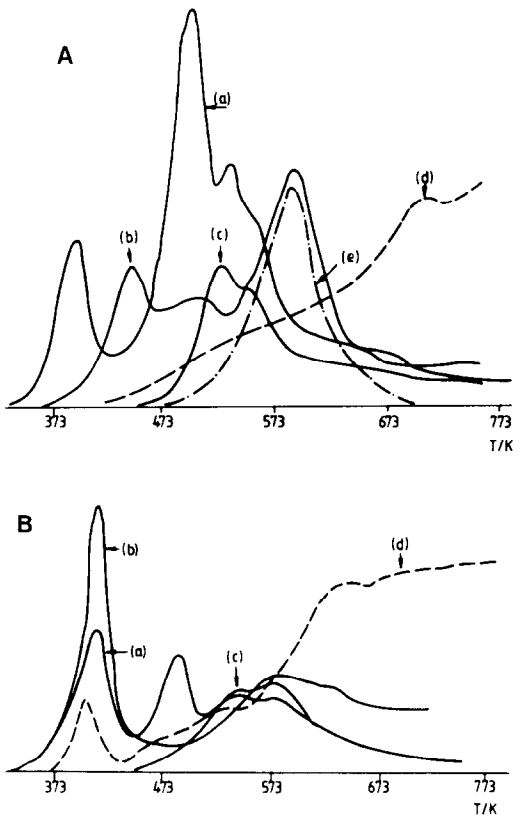

FIG. 9. Formation of H_2, CH_4, CO_2, and the overall decomposition curve for samples (II) (A) and (IV) (B) decomposed in helium and hydrogen. (a) Decomposition in H_2, (b) decomposition in He, (c) CH_4 formed in H_2, (d) H_2 formed in He (---), (e) CO_2 formed in He (- - - -).

(Fig. 9). On the contrary, for MCC with ruthenium in excess, the low temperature peak is missing, and at high temperature, in addition to methane and hydrogen, a broad CO_2 peak appeared (Fig. 9).

Previously (*1*) we suggested that the high dispersion and catalytic activity of catalysts prepared in helium are due to the presence of carbon left on the surface after decomposition. If this is so, the ratio *R* = carbon (meas.)/carbon (theor.) should be less than unity when the decomposition takes place in helium. In Table 6 values of carbon balance are summarized. The data show that these values tend to increase as ruthenium content increases from 0 to 100%. It is surprising, however, that when decomposition takes place in hydrogen the *R* values generally exceed the value of unity, i.e., the carbon balance is not correct.

In order to elucidate this, the GC–MS technique was applied. As a working hypothesis, we assumed that during the impregnation a trace amount of hexane is left on the impregnated Cab-O-Sil which is evacuated overnight. This is supported by the appearance of ir bands assigned to hydrocarbons (*1*). Indeed, when Cab-O-Sil alone was treated with hexane followed by the evacuation normally applied during the sample preparation, a small amount of hex-

TABLE 6

$R = \frac{\text{carbon (measured)}}{\text{carbon (theoretical)}}$ for Different MCC on Cab-O-Sil when Decomposed in Hydrogen and Helium[a]

			$Fe_3(CO)_{12}$	$Fe_2Ru(CO)_{12}$	$Fe_3(CO)_{12}$ $Ru_3(CO)_{12}$	$H_2FeRu_3(CO)_{13}$	$Ru_3(CO)_{12}$
H_2	770 K	TC	0.39	0.68 (0.14)[b]	1.05	1.48	1.70 (0.10)[b] (0.22)
	770 K	HC	0.35	0.40	—	0.62	1.08
	570 K	HC	—	—	—	0.33	—
He	770 K	TC	0.44	0.41 (0.34)	0.80 (0.37)	0.77 (0.24)	1.08 (0.9)
	570 K	TC	—	0.33	—	0.61	—
	770 K	HC	—	0.06	—	0.10	1.21
	570 K	HC	0.34	—	—	—	—

[a] Notation: TC: Total amount of carbon (in the form of CO, CO_2, CH_4)
HC: the amount of carbon formed in CH_4

[b] Numbers in parentheses denote the dispersion of the metal.

ane was observed in TPDC by the appearance of peaks of m/e = 57 and 43 around 350 K. However, when Cab-O-Sil contained $Ru_3(CO)_{12}$, a large methane peak appeared at around 500 K, preceded by peaks of m/e = 57 and 43 (Fig. 10). The most characteristic difference between Cab-O-Sil containing no Ru, and that containing $Ru_3(CO)_{12}$, is the large increase of CH_4 and CO_2 at temperatures above 630 K. When the preparation of Ru–MCC was carried out from a chloroform solution the high temperature CH_4 and CO_2 peaks are completely missing. These experiments clearly show the presence of carbon resulting from the decomposition of a trace amount of hexane left on Cab-O-Sil after impregnation. When TPDC occurs in hydrogen, hydrogenation of this carbon predominates, and thus the carbon balance exceeds the value of R = 1.

Temperature-programmed reaction (TPR) of carbon monoxide was applied as a test reaction for characterizing the catalytic activity of the decomposed samples presented in Fig. 11. Without any kinetic details the different samples decomposed in helium normally possess higher activity than those treated in hydrogen. On the other hand, the samples tend to appear less active, with increasing iron content, than

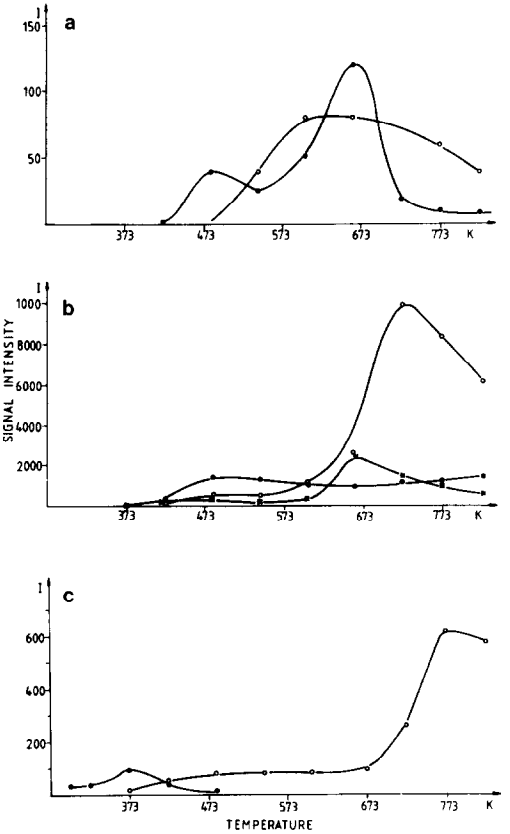

FIG. 10. GC–MS studies on Cab-O-Sil wetted by *n*-hexane (a), $Ru_3(CO)_{12}$ deposited on Cab-O-Sil from hexane (b), and chloroform (c) solution. (×) m/e = 16, (○) m/e = 44, (●) m/e = 57.

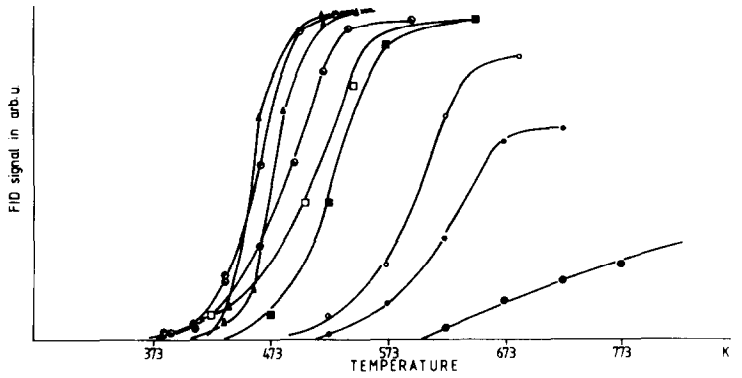

FIG. 11. TPR of CO in hydrogen on catalysts decomposed in helium and hydrogen. (○) sample (I) in He; (○) sample (II) in He; (●) sample (II) in H_2; (▲) sample (III) in H_2; (△) sample (III) in He; (□) sample (IV) in He; (■) sample (IV) in H_2; (◐) sample (V) in He; (◒) sample (V) in H_2.

sample (I). This general feature has also been observed in kinetic measurements (*17, 18*).

DISCUSSION

Generally speaking, a similar type of interaction was found for sample (I) and sample (V) (*1*) concerning the broadening and frequency shift for the C–O ir band. However, here the frequency shift is smaller than for iron dodecacarbonyl, which points to a weaker interaction. Bands above 2110 cm^{-1} can be related either to the CO molecule bonded to oxidized ruthenium atoms (*16*) or to the asymmetric modes of adsorbed twin CO groups (*19*). Here it is suggested that it is not twin CO groups, because the intensity increases with decreasing CO content.

On impregnation, interactions do not exist between $Ru_3(CO)_{12}$ and $Fe_3(CO)_{12}$, and the presence of ruthenium has no influence on iron up to 400 K, as indicated by the comparison of the Mössbauer spectra of iron and iron–ruthenium containing samples.

Here again, the stability of the metallic framework can be established, because when heating the sample to 400 K, CO readsorption, which restores the original surface species, can be observed.

The ir spectra recorded during decomposition give more detail on the mechanism. In contrast to the decomposition of sample (V), on sample (I) at least two species, different in CO content, can be distinguished. The plot in Fig. 12 shows this phenomenon. On curve (b) there are three break points at 340, 365, and 395 K, and accordingly, species containing less and less CO molecules are formed. This is supported by studying the ratio-recorded spectra (Fig. 13). Up to approximately 340 K, positive bands are characteristic of the original $Ru_3(CO)_{12}$/Cab-O-Sil, and part of the $Ru_3(CO)_{12}$ decomposes to $Ru_3(CO)_{12-n}$. The negative band shown at 2083 cm^{-1} is characteristic of the decomposition products left on the surface [see spectra (b), (c), (d), and (e) in Fig. 13].

The "negative" band may be attributed to a poorer hydrogenated surface carbonyl species. This assignment seems to be proven by the fact that only the Ru–carbonyls, namely, $H_2Ru_4(CO)_{13}$ (*3*) and α-$H_4Ru_4(CO)_{12}$ (*20*) showed strong bands in the 2070–2100 cm^{-1} range.

Above 340 K the $Ru_3(CO)_{12-n}$ species is decomposed, with further loss of CO, and a carbonyl-poor $Ru_3(CO)_{12-m}$ ($m > n$) surface intermediate is formed, which could be characterized by the 2080, 2072, and 2028 cm^{-1} bands.

The first two band doublets can be assigned to the spectra of ruthenium carbonyls containing carbon (*21*), although from

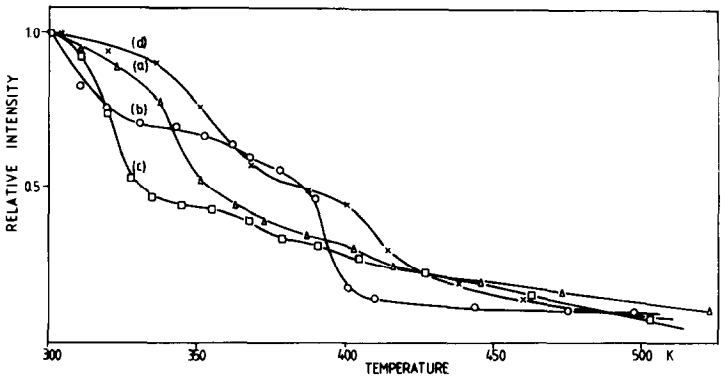

FIG. 12. Temperature dependence of relative band intensity of the most intense CO stretching band near 2065 cm^{-1} for (a) $[Ru_3(CO)_{12} + Fe_3(CO)_{12}]$/Cab-O-Sil (under vacuum), (b) $Ru_3(CO)_{12}$/Cab-O-Sil (under H_2), (c) $[Ru_3(CO)_{12} + Fe_3(CO)_{12}]$/Cab-O-Sil (under H_2), (d) $Ru_3(CO)_{12}$/Cab-O-Sil (under vacuum).

the metal–carbonyl ratio it can be concluded that the two bands near 2075 and 2030 cm^{-1} can be assigned to an intermediate surface species which preserves the cluster framework on the surface (see Scheme 1).

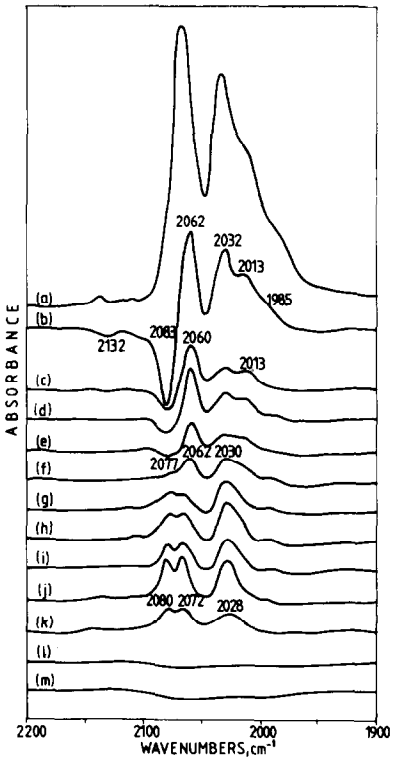

FIG. 13. Ratio-recorded spectra for $Ru_3(CO)_{12}$/Cab-O-Sil calculated from the spectra of Fig. 2. (a) Original cluster at 298 K; (b) 302/311 K; (c) 311/320 K; (d) 320/331 K; (e) 331/343 K; (f) 343/353 K; (g) 353/362 K; (h) 362/368 K; (i) 368/378 K; (j) 378/390 K; (k) 390/401 K; (l) 401/410 K; (m) 410/444 K.

Concluded that the two bands near 2075 and 2030 cm^{-1} can be assigned to an intermediate surface species which preserves the cluster framework on the surface (see Scheme 1).

This surface intermediate with C_{3v} symmetry is assumed because (i) it appears in the form of slightly split doubly-degenerate asymmetric (2080 and 2072 cm^{-1}) and symmetric (2028 cm^{-1}) stretching; (ii) Ru_3 frameworks appear to be present because on addition of CO, $Ru_3(CO)_{12-n}$ is formed again, and (iii) $Ru_3(CO)_3$ spectra show resemblance to those obtained for linearly bonded CO upon CO chemisorption on Ru/SiO_2 after recarbonylation.

Furthermore, it is difficult to believe that these two bands near 2075 and 2030 cm^{-1} belong to twin CO as stated by Zecchina *et al.* (*8*) for Al_2O_3 support, because the relative intensity increases with diminishing CO coverage in certain temperature ranges.

However, the absorption bands at 2080, 2072, and 2028 cm^{-1} may correspond to the strongest bands in the spectrum of

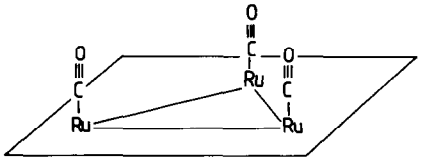

SCHEME 1

TABLE 7

Averaged[a] CO Stretching Force Constants for "Free"[b] and Supported Clusters

Cluster	$\bar{\nu}^a$ (cm^{-1})	K(CO)	F(CO,CO)	n(CO)	n(MC)
		(10^2 N m^{-1})			
$Ru_3(CO)_{12}$[b]	2030.9[c]	16.67	0.40	2.70_8	1.29_2
$Ru_3(CO)_{12}$/Cab-O-Sil	2032.2[d]	16.69	0.82	2.71_1	1.28_9
$Fe_3(CO)_{12}$[b]	2029.3[d]	16.64_5	0.54	2.70_4	1.29_6
	1868[e]	13.84	0.26	2.27	1.73[f]
	1833[e]				
$Fe_3(CO)_{12}$ on Cab-O-Sil	2037.7[d]	16.78	0.74	2.72_5	1.27_5
	1869[e]	13.64	0.48	2.24	1.76[f]
	1805[e]				

[a] Averaged ir stretching frequencies.
[b] *n*-Hexane solution data.
[c] Ref. (*24*).
[d] Ref. (*1*).
[e] Actual frequencies.
[f] Value for two bridging MC bonds.
Note. K, CO stretching and F, stretch–stretch interaction force constant; n, bond order calculated from K(CO), (*25*).

$H_4Ru_4(CO)_{12}$ which readily formed from $Ru_3(CO)_{12}$ by interaction with hydrogen in octane at 363 K (*22*). In presence of CO this reaction can be reversed and equilibrium exists among $Ru(CO)_5$, $Ru_3(CO)_{12}$, and $H_4Ru_4(CO)_{12}$ (*23*). Since the spectra observed here were recorded after most of the CO has left the molecule, this explanation can be omitted.

In spectra (g)–(k) in Fig. 13 further decomposition of $Ru_3(CO)_3$ surface can be observed in the temperature range of 360 to 410 K. Spectrum (1) shows the end of decomposition.

A simplified force constant calculation has also been performed for the investigated metal–carbonyl clusters (Table 7). The CO stretching force constants, calculated from the averaged infrared active frequencies of terminal CO groups, are only slightly higher in the supported state than those in *n*-hexane solution. Stronger increases were observed in stretch–stretch interaction terms. The absolute values of these latter force constants are slightly overestimated by the simplified calculation used. A more complete force constant calculation for $Ru_3(CO)_{12}$ gave the average (axial and equatorial) K(CO) equal to 16.66×10^2 N m^{-1} (*5*). The K(CO) value for $Fe(CO)_5$ is 16.7×10^2 N m^{-1} (*26*). These values are reasonably close to those in Table 7. As seen in this table, cluster–support interaction for $Fe_3(CO)_{12}$ strengthens the terminal CO bonds, while those of bridged CO are weakened.

In the case of mixtures more complex features are revealed. Ratio-recorded spectra on sample (III) decomposed in hydrogen are presented in Fig. 14. It can be established that at the beginning of decomposition mainly $Fe_3(CO)_{12}$ is decomposed [(a) to (d)]. In spectrum (e) decomposition of $Ru_3(CO)_{12}$ also commences, while in spectra (f), (g), and (h) the formation of $Ru_3(CO)_3$ surface species can be observed. In spectrum (i) the characteristic band of chemisorbed CO can be seen.

On the basis of curves (b) and (c) in Fig. 12, a qualitative comparison can be made in the decomposition rate of the two systems. When $Fe_3(CO)_{12}$ is present, decomposition is accelerated, whereas above 400 K CO is significantly retained. From curve (a) in Fig. 12, one may infer that in decomposition occurring in vacuum the overall pro-

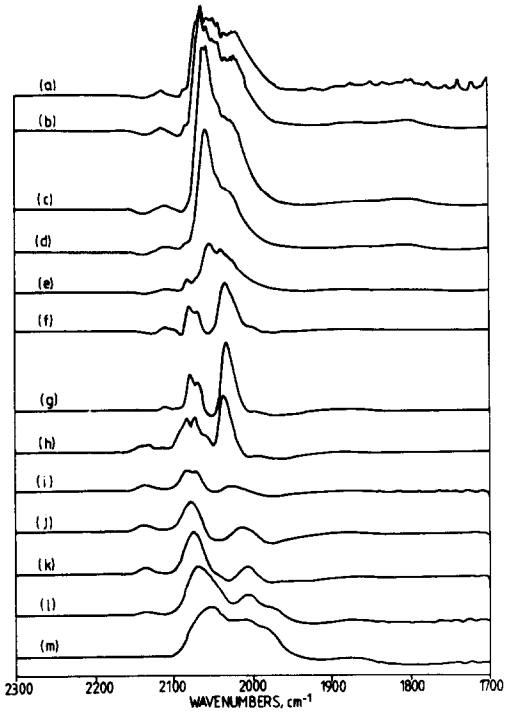

FIG. 14. Ratio-recorded spectra for $Fe_3(CO)_{12}$ + $Ru_3(CO)_{12}$ on Cab-O-Sil calculated from Fig. 5. (a) 301/311 K; (b) 311/319 K; (c) 319/328 K; (d) 328/335 K; (e) 335/345 k; (f) 345/355 K; (g) 355/368 K; (h) 368/379 K; (j) 391/405 K; (k) 405/428 K; (l) 428/463 K; (m) 463/503 K.

cess is retarded in comparison to that occurring in H_2.

The ratio-recorded spectra of sample (III) decomposed in vacuum are very similar to those obtained in H_2 (see Fig. 15). However, at 470–570 K a new type of decomposition commences, characterized by the bands at wavenumbers of 2127 w, 2090 sh, 2070 s, 2042 s, 2007 s, and 1952 m. Since carbon is left on the surface, this phenomenon may be interpreted by the presence of carbon, which may affect the spectra of the chemisorbed CO.

Since bridged CO (1862 and 1805 cm^{-1}) behaved exactly in the same way for sample (III) and (V), it can be established that the presence of $Ru_3(CO)_{12}$ does not influence the decomposition of $Fe_3(CO)_{12}$. However, $Ru_3(CO)_{12}$ decomposition was significantly modified by the presence of iron.

Infrared measurements have indicated that interaction between iron and ruthenium starts during decomposition at low temperature. These data, however, give no information about the metal–metal interaction at higher temperature. Investigations of iron–ruthenium coimpregnated samples by Mössbauer spectroscopy have indicated the presence of interaction between the two metals. At low Fe/Ru ratios and high total metal loading, significant interaction was detected; Ru enhanced the reduction of iron on samples prepared by the incipient wetness techniques (*27*). At low metal loadings and higher Fe/Ru ratios, ruthenium was reported to inhibit the reduction (*28*). In our case, at low metal loading and higher Fe : Ru ratio on samples prepared from coimpregnated carbonyls, the reduction was also promoted by ruthenium: a part of iron was reduced to the zero-valent state

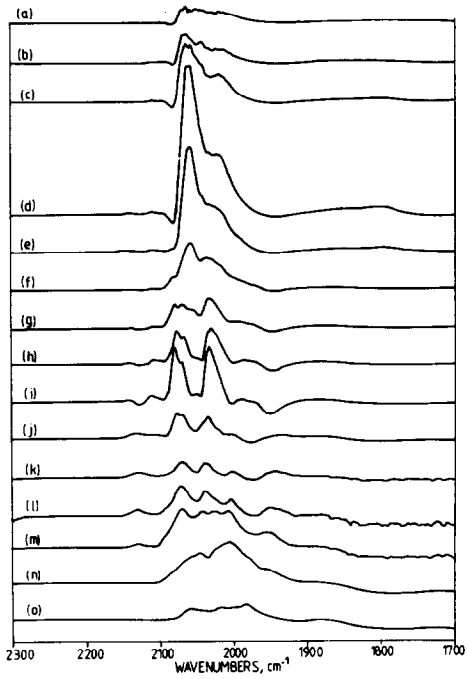

FIG. 15. Ratio-recorded spectra for $Fe_3(CO)_{12}$ + $Ru_3(CO)_{12}$ on Cab-O-Sil calculated from spectra in Fig. 7. (a) 298/311 K; (b) 311/323 K; (c) 323/338 K; (d) 338/351 K; (e) 351/363 K; (f) 363/373 K; (g) 373/387 K; (i) 403/416 K; (j) 416/446 K; (k) 446/473 K; (l) 473/523 K; (m) 533/573 K; (n) 573/623 K; (o) 623/673 K.

(Table 4). This is the main difference between preparations using metal–carbonyl clusters and inorganic salt solutions for impregnation.

Results obtained from measurements on iron–ruthenium samples treated in helium were similar to those found on pure iron. Comparison of Figs. 6(b) and (c) clearly shows the presence of a reducing process when the sample is heated to 670 K without hydrogen.

At this stage of the discussion, some general features can be shown concerning the decomposition of the clusters. Generally, the decomposition can be divided into two parts: (i) at low temperatures (up to 400 K) only primary decomposition occurs, accompanied by the elimination of CO and the partial oxidation of iron and possibly ruthenium on the surface; and (ii) at high temperatures (>400 K) secondary reactions take place, in this case the formation of the metallic phase, i.e., the creation of the supported metal catalyst occurs. The secondary processes are characterized by the presence of surface carbon hindering the agglomeration and migration of small metallic particles to form large crystallites. Due to the interaction of surface carbon with the OH groups of the silica support and catalysed by the metallic particles, the surface carbon is partially removed from the surface, producing secondary products such as H_2O (*16*), CO_2, CH_4 and H_2.

The overall mechanism for decomposition of samples (I) and (V) is different because CO molecules leave the cluster in one step in (V) but gradually in (I). The small metal particles on the surface are oxidized in the reaction proposed by Dutartre *et al.* (*29*):

$$Fe^0 + H^+ = Fe^+ + \tfrac{1}{2}H_2 \qquad (1)$$

Although this reaction was assumed to occur at higher temperature and at higher metal loading, here the metal particles formed are thermodynamically unstable, and Reaction (1) can proceed at lower temperature, using the OH groups of Cab-O-Sil. The small H_2 peak appearing at low temperature also indicates this reaction. Of course, when the temperature is increased the reaction proceeds faster, which results in the large amount of hydrogen shown in Fig. 9.

In addition to the formation of Fe^{2+} and Fe^{3+}, the surface is also partly covered by carbon. (The disappearance of the CO stretching frequency is not evidence for the removal of total carbon.) This reaction is responsible for the small amount of hydrogen formation at low temperature on sample (V). At higher temperatures, the structural OH groups commence to react with carbon:

$$2C_{(surf)} + 2OH_{(structural)} = 2CO + H_2 \qquad (2)$$

and thus the formation of H_2 at higher temperature is explained. The reactivity of OH groups on silica has been shown (*31*). The process described by Reaction (2) is characteristic also of sample (I). The hydrogen produced in Reaction (2) can be used for the hydrogenation of carbon, which appears in the form of methane. On sample (V) CO_2 formation was not detected, whereas on sample (I) this process is predominant at high temperature. This difference reveals weaker Ru–O bonds which can easily react with the CO formed in Reaction (2):

$$O_{surf} + CO = CO_2 \qquad (3)$$

The CO shift reaction cannot be neglected, either, that is,

$$CO + H_2O_{(structural)} = CO_2 + H_2 \qquad (4)$$

All of these reactions contribute to the removal of surface carbide and oxide, especially from ruthenium or RuFe. The formation of metallic particles, capable of adsorbing CO, is indicated by the high dispersion of samples (I) and (III). Since iron is covered by oxides and carbides, CO adsorption is diminished, although at the reaction temperature, the adsorption of CO and

the subsequent formation of active carbon species can also be detected (*31*).

Interaction of surface carbon with hydrogen is shown by the methane formation in the medium (470–570 K) and high (>570 K) temperature range on ruthenium-rich samples. Metallic ruthenium, in the presence of hydrogen, is a good hydrogenolysis catalyst (*32*), i.e., the hexane moieties adsorbed on the carrier can be easily hydrogenolyzed, resulting in the formation of CH_4. Nevertheless, CO dissociates easily on supported ruthenium, while on iron-containing samples some of the CO is in molecular form (*33*). This shows the Ru–Fe interaction again.

From the ir and Mössbauer data presented here, it is now clear that interaction between $Fe_3(CO)_{12}$ and $Ru_3(CO)_{12}$ in the impregnated phase either does not exist, or is very weak. It develops later, after decomposition, and this starts with the decomposition of $Fe_3(CO)_{12}$. This may explain why the Mössbauer spectra of sample (III) and (V) are very similar during the decomposition, up to 420 K, regardless of the atmosphere (He or H_2) in which the decomposition takes place. The ferrous oxide phase formed acts as stabilizer for the ruthenium formed by decomposition. This mechanism has been proposed by Topsøe *et al.* for the Fe/MgO system (*34*) and by Guczi *et al.* (*28*) for $FeRu/SiO_2$ catalysts. The highly dispersed state of iron and ruthenium ensures the reduction of iron at 470 K, which is not possible for FeRu prepared from $RuCl_3$ and $Fe(NO_3)_3$ (*28*).

The highly dispersed surface carbon, originating either from CO dissociation in He or from the cracking of the solvent moieties, acts as a stabilizing agent for the metallic particles as is clearly indicated by the enhanced CO adsorption (*2*). In addition, even when pure iron is treated with hydrogen, the carbon can eventually be removed. The metallic particles then coagulate into large, ferromagnetic iron particles.

Adsorption, as well as temperature-programmed reaction, of CO reflects the features of the catalytic properties. Normally the presence of ruthenium in the sample increases the number of metallic sites, which increases the amount of CO chemisorbed. Simultaneously, catalysts prepared from ruthenium-containing MCC are also more active than those prepared from iron-rich ones. Within this series, samples decomposed in helium always show higher activities than those decomposed in hydrogen. This behavior is the result of the removal of surface carbon in the presence of hydrogen, which in turn results in the formation of large metallic particles.

ACKNOWLEDGMENTS

The authors are indebted to Mr. I. Bogyay and Mrs. M. Klug for technical help in carrying out TPDC, TPR, and infrared measurements.

REFERENCES

1. Lázár, K., Matusek, K., Mink, J., Dobos, S., Guczi, L., Vizi-Orosz, A., Markó, L., and Reiff, W. M., *J. Catal.*, **87,** 179 (1984).
2. Kuznetsov, V. L., Bell, A. T., and Yermakov, Yu. I., *J. Catal.* **65,** 374 (1980).
3. Guczi, L., Schay, Z., *React. Kinet. Catal. Lett.* **14,** 207 (1980).
4. Ballivet-Tkatchenko, D., Coudurier, G., Tkatchenko, I., Figueiredo, C., *Prepr. Div. Pet. Chem. Amer. Chem. Soc.* **25,** 755 (1980).
5. Hugues, F., Smith, A. K., Ben Taarit, Y., Basset, J. M., Commereuc, D., and Chauvin, Y., *J. Chem. Soc. Chem. Commun.* 68 (1980).
6. Goodwin, J. G., and Naccache, C., *J. Mol. Catal.* **14,** 259 (1982).
7. Knözinger, H., Zhao, Y., Tesche, B., Barth, R., Epstein, R., Gates, B. C., and Scott, J. P., *Discuss. Faraday Soc.* **72,** 53 (1982).
8. Zecchina, A., Guglielminotti, E., Bossi, A., and Camia, N., *J. Catal.* **74,** 225 (1982).
9. Guglielminotti, E., Zecchina, A., Bossi, A., and Camia, N., *J. Catal.* **74,** 240 (1982).
10. Guglielminotti, E., Zecchina, A., Bossi, A., and Camia, N., *J. Catal.* **74,** 252 (1982).
11. Bilhou, J. L., Bilhou-Bougnol, V., Craydon, W. F., Basset, J. M., Smith, A. K., and Zanderighi, G. M., *J. Organomet. Chem.* **153,** 73 (1978).
12. Smith, A. K., Hugues, F., Theolier, A., Basset, J. M., Ugo, R., Zanderighi, G. M., Bilhou, J. L., Bilhou-Bougnol, V., and Craydon, W. F., *J. Inorg. Chem.* **18,** 3104 (1979).

13. Theolier, A., Smith, A. K., Leconte, M., Basset, J. M., Zanderighi, G. M., Psaro, R., and Ugo, R., *J. Organomet. Chem.* **191,** 415 (1980).
14. Yawney, D. B. W., and Stone, F. G. A., *J. Chem. Soc. A* 502 (1969).
15. Brown, M. F., and Gonzalez, R. D., *J. Phys. Chem.* **80,** 1731 (1976).
16. Guczi, L., Schay, Z., Matusek, K., Bogyay, I., and Stefler, G., "Proceedings, 7th International Congress on Catalysis (Tokyo 1980)," p. 211, Kodansha/Tokyo, Elsevier/Amsterdam, 1981.
17. Guczi, L., Schay, Z., Lázár, K., Vizi, A., and Markó, L., *Surf. Sci.* **106,** 516 (1981).
18. Schay, Z., and Guczi, L., *Acta Chim. Acad. Sci. Hung.* **111,** 597 (1982).
19. Dalla Betta, R. A., *J. Phys. Chem.* **79,** 2519 (1979).
20. Johnson, B. F. G., Johnston, R. D., Lewis, J., and Robinson, B. H., *J. Chem. Soc. (A)* 2856 (1968).
21. Johnson, B. F. G., Lewis, J., and Williams, I. G., *J. Chem. Soc.* 901 (1970).
22. Kaesz, H. D., Knox, S., Koepke, J. W., and Saillant, R. B., *J. Chem. Soc. Chem. Commun.* 477 (1971).
23. Piacenti, F., Bianchi, M., Frediani, P., and Benedetti, E., *Inorg. Chem.* **10,** 2759 (1971).
24. Battiston, G. A., Bor, G., Dietler, U. K., Kettle, S. F., Rosetti, R., Sbrignadello, G., and Stanghellini, P. L., *Inorg. Chem.* **19,** 1961 (1980).
25. Goggin, P. L., and Mink, J., *Inorg. Chim. Acta* **34,** 225 (1979).
26. Bor, G., *Inorg. Chim. Acta* **3,** 191 (1969).
27. Vannice, M. A., Lam, Y. L., Garten, R. L., *Advan. Chem.* **178,** 25 (1979).
28. Guczi, L., Matusek, K., Eszterle, M., Manninger, I., and Király, J., "Preparation of Catalysts II," p. 391. Elsevier, Amsterdam, 1979.
29. Dutartre, R., Bussière, P., Dalmon, J. A., and Martin, G. A., *J. Catal.* **59,** 382 (1979).
30. Guczi, L., and Till, F., Mater. Sci. Monographs, No. 10, p. 908. Elsevier, Amsterdam, 1982.
31. Lázár, K., Schay, Z., and Guczi, L., *J. Mol. Catal.* **17,** 205 (1982).
32. Sinfelt, J. H., "Advances in Catalysis," Vol. 23, p. 91. Academic Press, New York, 1973.
33. Brenner, A., *J. Chem. Soc. Chem. Commun.* 1979, 251.
34. Topsøe, H., Dumesic, J. A., Derouane, E. G., Clausen, B. S., Mørup, S., Villadsen, J., and Topsøe, N., "Preparation of Catalysis II," p. 365. Elsevier, Amsterdam, 1979.